NSCLC Extracellular Vesicles Containing miR-374a-5p Promote Leptomeningeal Metastasis by Influencing Blood–Brain Barrier Permeability

Jie Jin[1,2,3], Yumeng Cui[2], Huicong Niu[4], Yanli Lin[2], Xiaojie Wu[2], Xuejiao Qi[1,5], Kaixuan Bai[1,5], Yu Zhang[1,5], Youliang Wang[2], and Hui Bu[1,5]

ABSTRACT

Leptomeningeal metastasis (LM) is a devastating complication of advanced non–small cell lung cancer (NSCLC). Its diagnosis and monitoring can be challenging. Recently, extracellular vesicle (EV) miRNAs have become a new noninvasive diagnostic biomarker. The purpose of this study was to examine the clinical value and role of EV miRNAs in NSCLC-LM. Next-generation sequencing analysis revealed that miRNAs with differential expression of EVs in sera of patients with NSCLC with LM and non-LM were detected to identify biological markers for the diagnosis of LM. Cellular and *in vivo* experiments were conducted to explore the pathogenesis of EV miRNA promoting LM in NSCLC. In the present study, we first demonstrated that the serum level of EV-associated miR-374a-5p in patients with LM of lung cancer was much higher than that in patients without LM and was correlated with the survival time of patients with LM. Further studies showed that EV miR-374a-5p efficiently destroys tight junctions and the integrity of the cerebral microvascular endothelial cell barrier, resulting in increased blood–brain barrier permeability. Mechanistically, miR-374a-5p regulates the distribution of ZO1 and occludin in endothelial cells by targeting γ-adducin, increasing vascular permeability and promoting LM.

Implications: These results suggest that serum NSCLC–derived EV miR-374a-5p is involved in premetastatic niche formation by regulating the permeability of the blood–brain barrier to promote NSCLC-LM and can be used as a blood biomarker for the diagnosis and prognosis of NSCLC-LM.

Introduction

Leptomeningeal metastasis (LM) is a terminal stage with devastating consequences to patients with cancer. LM occurs in approximately 5% to 10% of patients with solid tumors, and this percentage is expected to increase. The majority of LMs are derived from breast cancer, melanoma, and lung cancer (1). LM occurs in 3% to 5% of patients with advanced non–small cell lung cancer (NSCLC; ref. 2). Patients with EGFR mutations were more frequent to develop LM than those with wild-type EGFR (9.4% vs. 1.7%; ref. 3). The prognosis for LM is extremely poor, with a median overall survival time of only 3.6 to 12 months (4). Therefore, it is crucial to diagnose LM early and provide the patient with the best chance of treatment.

However, diagnosis of LM can be challenging. Most symptoms and signs of patients with LM are nonspecific owing to the involvement of different central nervous system areas and cannot alone justify a diagnosis of LM (5). At present, the diagnosis of LM mainly relies on MRI and cerebrospinal fluid (CSF) cytology, but their sensitivity is low (6, 7). MRI findings of various diseases involving the leptomeningeal structures are similar to those of LM, with little distinctive capacity between some diseases and LM (8, 9). CSF cytology remains the gold standard for the diagnosis of LM. However, a drawback of CSF cytology is the low sensitivity of 68%. To improve sensitivity, repeated CSF sampling is required for analysis (10). It is imperative for LM to provide convenient diagnostic methods.

Extracellular vesicles (EV) have received increasing attention as biomarkers for tumor diagnosis (11). EVs are membranous vesicles secreted by cells and can be roughly divided into three categories: apoptotic bodies, microvesicles, and exosomes (12). The function of EVs depends on the various contents that they carry, which include proteins, lipids, and various types of nucleic acids (13). EVs are used as a cancer biomarker because of several advantages. First, EVs are widely distributed in body fluids (including urine, blood, and CSF) and are easy to extract. Second, tumor-derived EVs carry functional molecular cargo from the original cells and are specific. Finally, EVs are lipid bilayer–enclosed structures, which can protect the biological activity of the cargo and have strong stability (14). Studies have shown that tumor-derived EVs can be used as markers of bone (15), liver (16), brain (17), and lymphatic metastases (18) of lung cancer. However, studies on NSCLC-LM are extremely rare.

In this study, we demonstrated that miR-374a-5p is specifically upregulated in serum EVs of patients with NSCLC-LM. EV miR-374a-5p levels were negatively correlated with the prognosis of patients. Experiments showed that NSCLC cell–derived EV miR-374a-5p could promote NSCLC-LM. The mechanism involves the transfer of miR-374a-5p to human microvascular endothelial cells through EVs and

[1]The Second Hospital of Hebei Medical University, Shijiazhuang, PR China. [2]Beijing Institute of Biotechnology, Beijing, PR China. [3]Xiong'an Xuanwu Hospital, Baoding, PR China. [4]Department of Neurology, Minhang Hospital, Fudan University, Shanghai, PR China. [5]Key Laboratory of Clinical Neurology, Ministry of Education, Shijiazhuang, PR China.

J. Jin and Y. Cui contributed equally to this article.

Corresponding Authors: Youliang Wang, Beijing Institute of Biotechnology, Beijing 100071, PR China. E-mail: wang_you_liang@aliyun.com; and Hui Bu, The Second Hospital of Hebei Medical University, Shijiazhuang 050000, PR China. E-mail: 26500825@hebmu.edu.cn

Mol Cancer Res 2024;22:699–710

doi: 10.1158/1541-7786.MCR-24-0052

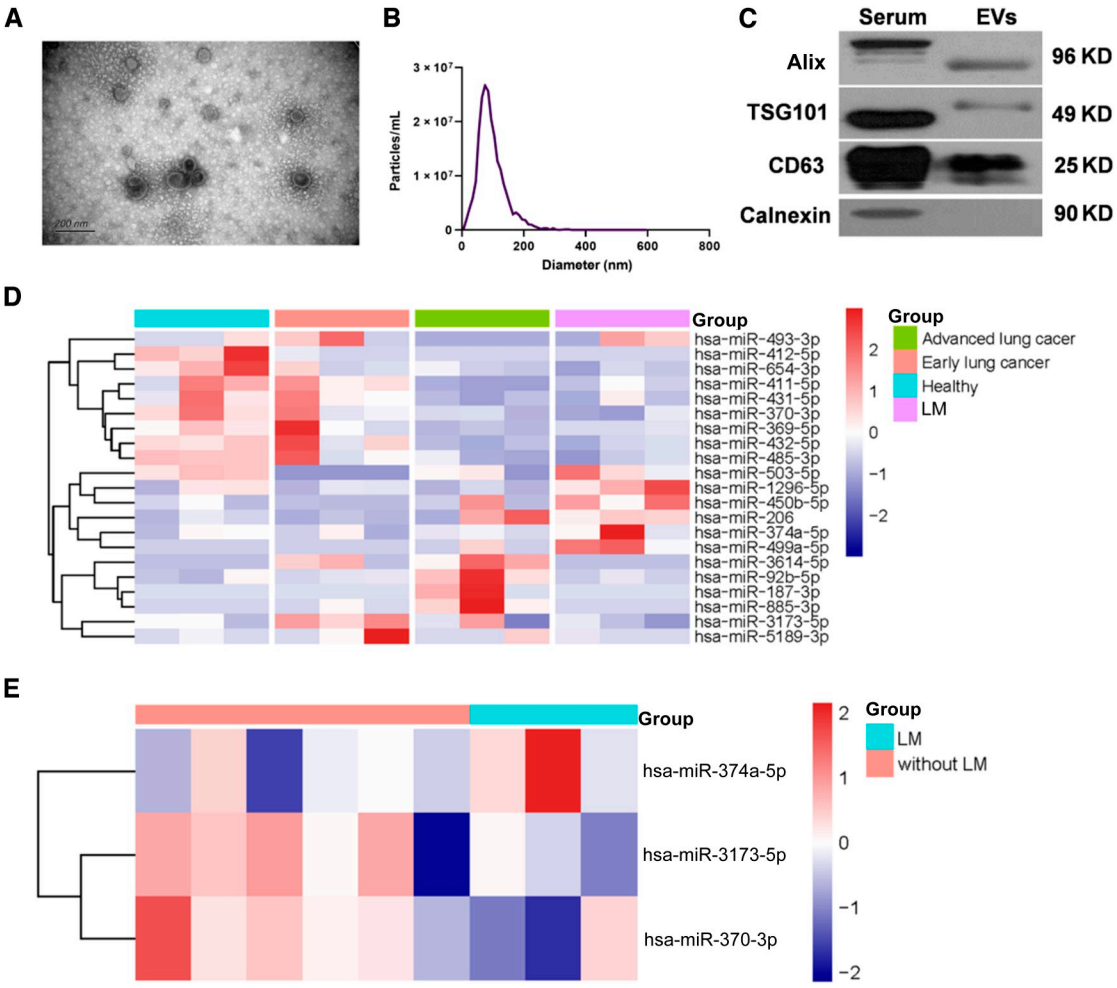

Figure 1.

NGS of EV miRNA in serum. **A,** TEM of EVs derived from serum. Scale bar represents 200 nm. **B,** NTA shows that the particle size of EVs ranges from 30 to 150 nm. **C,** WB analysis of TSG101, CD63, Alix, and calnexin in serum EVs. **D,** Heatmap of miRNA profiles in serum EVs of nontumor, early NSCLC, advanced NSCLC (without LM), and NSCLC-LM samples. **E,** The NGS data of serum EVs miRNAs were divided into NSCLC-LM and non-LM analyses of specific expression of miRNAs.

promotes blood–brain barrier (BBB) permeability by targeting γ-adducin (ADD3) to enhance LM. Our findings suggested that NSCLC-derived serum EV miR-374a-5p may be considered a biomarker and promising target for the diagnosis and prognosis of LM.

Materials and Methods

Small RNA library preparation and sequencing

Total RNA was extracted and purified from EVs using the miRNeasy mini kit (QIAGEN, cat. no. 217004), according to the kit instructions. Then, sequencing libraries were generated using the NEBNext Multiplex Small RNA Library Prep Set for Illumina (NEB) following the manufacturer's recommendations, and index codes were added to attribute sequences to each sample. The libraries were then sequenced using an Illumina HiSeq 2500 instrument (Illumina).

Clinical samples

A total of 106 serum samples (including 30 noncancer, 24 early NSCLC, 26 advanced NSCLC without LM, and 26 NSCLC-LM samples) and 58 CSF samples (including 25 noncancer and 33 NSCLC-LM samples) were collected from The Second Hospital of Hebei Medical University. Written informed consent was obtained from all patients. This study was approved by the Ethics Committee of The Second Hospital of Hebei Medical University.

Cell lines

Human lung cancer cell lines (NCI-H1299, A549, 95C, and 95D) and immortalized human bronchial epithelial cells (BEAS-2B) were purchased from the ATCC. Immortalized human cerebral microvascular endothelial cells (hCMEC/D3), human normal astrocytes (HA1800), and human brain vascular pericytes (HBVPC) were purchased from the Shanghai Cell Bank. All cells were maintained at 37°C under 5% CO_2 with at least 95% humidity. hCMEC/D3 cells were cultured in endothelial cell medium (ECM) with 5% FBS (ScienCell). Other cell lines were cultured in DMEM (Gibco) with 10% FBS (HyClone). Cell lines were authenticated by routinely testing negative for *Mycoplasma* (November 30, 2019).

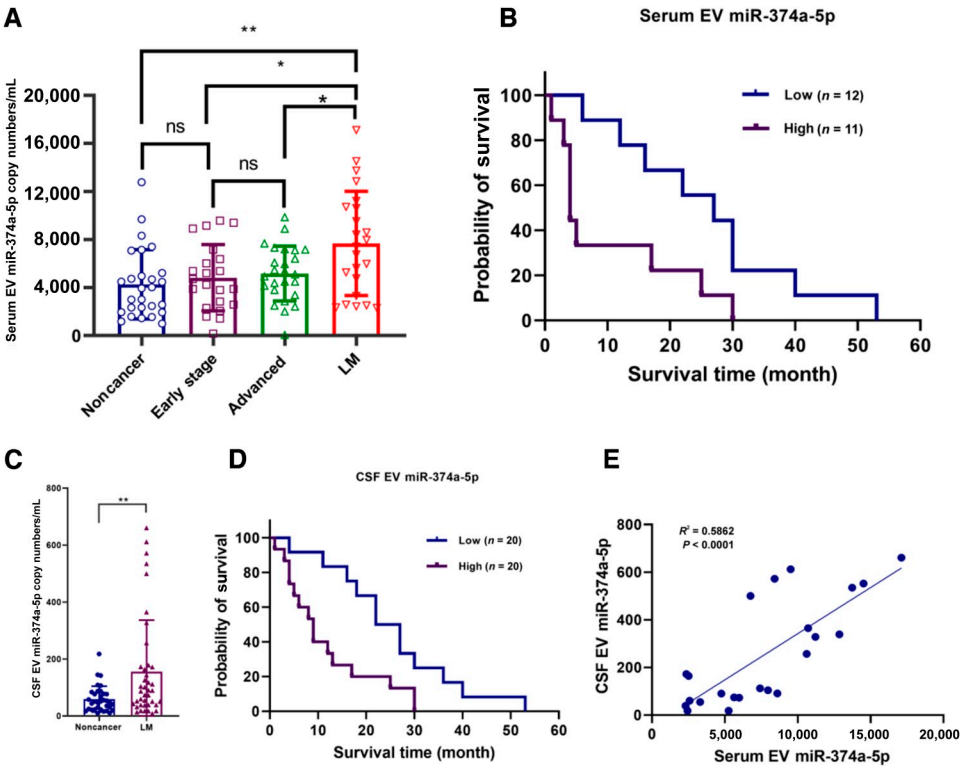

Figure 2.

The expression of EV miR-374a-5p was detected in serum and CSF. **A,** ddPCR quantified serum EV miR-374a-5p. The level of EV miR-374a-5p in serum of patients with NSCLC-LM was higher than that in patients with early and advanced NSCLC and more significant than that in noncancer samples. There was no difference in EV miR-374a-5p expression between noncancer, early, and advanced NSCLC. **B,** Serum EV miR-374a-5p was negatively correlated with survival time. **C,** ddPCR quantified CSF EV miR-374a-5p. The level of EV miR-374a-5p in NSCLC-LM was significantly higher than that in noncancer. **D,** CSF EV miR-374a-5p was negatively correlated with survival time. **E,** The EV miR-374a-5p levels were consistent between the CSF and the corresponding serum of patients with LM. *, $P < 0.05$; **, $P < 0.01$; ***, $P < 0.001$; ns, not significant.

EV isolation

Size-exclusion chromatography was used to isolate exosomes from serum and CSF. Specifically, 1 mL of the 0.8-μm–filtered samples was diluted with 1.5-fold PBS and purified using Exosupur columns (Echobiotech). The samples were eluted with 0.1 mol/L PBS according to the instructions, and 2 mL of the target fraction was collected. Finally, the collected exosome fraction with a molecular weight of 100 kDa was concentrated to 200 μL using the Amicon ultrafiltration tube (Merck).

Nanoparticle tracking analysis

The particle size and concentration of exosome solution with a particle concentration from 1×10^7/mL to 1×10^9/mL were detected using ZetaView PMX 110 (Particle Metrix), and the video duration of 60 seconds was shot with the excited light wave at 405 nm and the frame rate of 30 frames/second. Particle trajectories were analyzed using nanoparticle tracking analysis (NTA) software (ZetaView 8.02.28) to obtain the size and concentration of exosomes. NanoStandard of 100 nm (Applied Microspheres) was used for calibration during the NTA.

Transmission electron microscopy

The exosome sample was adjusted to the appropriate concentration, and 15 μL of the sample was absorbed and left for 2 minutes on the copper mesh. Then, a pipette gun was used to absorb about 15 μL of 2% uranyl acetate dyeing solution at room temperature for 1 minute and dried under an incandescent lamp for 3 minutes. The shape and size of exosomes were observed by transmission electron microscopy (TEM; H-7650, Hitachi Ltd.), and their photographs were taken.

Western blot analysis

Total proteins were extracted with RIPA lysis buffer (Thermo Fisher Scientific) and quantified using the Pierce BCA protein detection kit (Thermo Fisher Scientific). Protein concentrations were determined using the BCA protein assay kit (Thermo Fisher Scientific). Total protein was isolated by SDS-PAGE and transferred to a polyvinylidene difluoride membrane (Millipore) and then incubated with Abs (TSG101, Abcam; Alix, Abcam; CD63, Abcam; calnexin, Abcam; ADD3, Abcam; ZO1, Abcam; and occludin, Abcam). The membranes were then incubated with a secondary Ab (GAPDH, Cell Signaling Technology). The protein signal was visualized using a chemiluminescence system (Bio-Rad).

RNA preparation and qRT-PCR

RNA was extracted from cells using the Ambion PureLink total RNA kit (Invitrogen). RNA was quantified using a NanoDrop 1000 spectrophotometer (NanoDrop Technologies) and diluted to the same concentration. RNA was converted to cDNA using the Mir-X miRNA First-Strand Synthesis kit (Takara). cDNA was amplified on the CFX96 real-time PCR system (Bio-Rad) using THUNDERBIRD SYBR qPCR mix (TOYOBO). GAPDH and U6 were used as controls, and the $2^{-\Delta\Delta Ct}$ method was used for calculation.

Droplet digital PCR

The reaction system for droplet digital PCR (ddPCR) was prepared using QX200 ddPCR EvaGreen supermix according to the manufacturer's instructions. After PCR amplification, the information for samples in the 96-well plate was set and analyzed using QuantaSoft software.

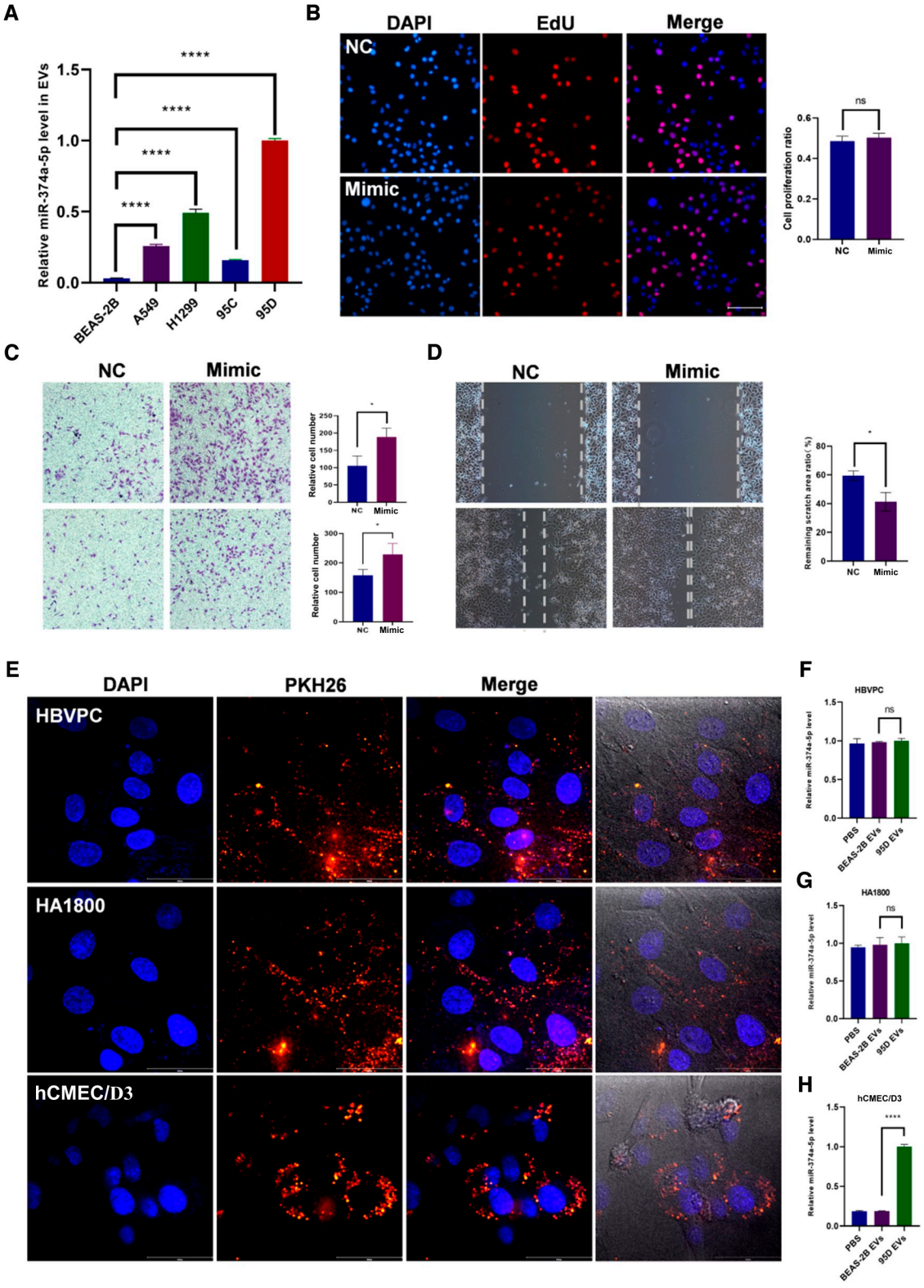

Figure 3.

EV miR-374a-5p was absorbed by brain microvascular endothelial cells. **A,** Expression of miR-374a-5p in EVs derived from a normal bronchial epithelial cell line (BEAS-2B) and NSCLC cell lines (A549, H1299, 95C, and 95D) by qRT-PCR. **B,** EdU assays detecting A549 cell viability (*Continued on the following page.*)

5-Ethynyl-2′-deoxyuridine assay

The cells were inoculated on a slide, and 10 μmol/L 5-ethynyl-2′-deoxyuridine (EdU) was added. The experiment was performed using the BeyoClick EdU cell proliferation kit (Beyotime). According to the manufacturer's protocol, the cells were stained with Alexa Fluor 594 and 4',6-diamidino-2-phenylindole (DAPI) and then photographed and recorded using a fluorescence microscope (Nikon). The cell proliferation rate was calculated as EdU-positive nuclei/total nuclei.

Transwell migration and invasion assays

Both migration and invasion assays were performed with a Transwell pore polycarbonate membrane insert (Corning), with the difference that Matrigel was added to the upper chamber of the invasion assay. The cells were inoculated in the upper chamber and cultured with the serum-free medium. A medium containing 10% FBS was added to the lower chamber. After 24 hours, the insertion was soaked in methanol to fix the cells and then stained with crystal violet for 20 minutes. The insert was washed with PBS to remove cells from the upper membrane. Images of stained cells were captured using a microscope (Nikon).

Endothelial tube formation assay

Matrigel (BD Biosciences) was added to a 24-well plate to form a flat surface. After the solidification of the gel, vascular endothelial cells were seeded into the wells and photographed using an inverted phase-contrast microscope.

Immunofluorescence

Cells seeded on coverslips were fixed with 4% paraformaldehyde, and FBS was added dropwise for blocking. Then, the cells were incubated with anti-ZO1 (Abcam) and anti-occludin (Abcam) Abs. Subsequently, the cells were incubated with a fluorescent secondary Ab. DAPI was added to stain nuclei. Images were acquired under a fluorescence microscope.

Dual luciferase reporter assay

The 3′–untranslated region (3′-UTR) of *ADD3* was subcloned and inserted into the psiCHECK-2 vector (Promega). In the mutant psiCHECK-2 vector, the miR-374a-5p–binding site in the 3′-UTR of *ADD3* was mutated. Cells were transfected with these vectors and the Renilla expression plasmid using Lipofectamine 2000 (Thermo Fisher Scientific catalog number:11668019) in a 24-well plate. Twenty-four hours after transfection, the cells were lysed with passive lysis buffer (Promega), and reporter expression was evaluated using a dual luciferase reporter assay system (Promega).

In vivo metastasis experiments

In vivo experiments were conducted using female nu/nu mice ages 6 weeks. First, EVs were injected into the caudal vein once every other day for a total of seven injections. Lewis lung cancer cells (LLC) were then injected into the left ventricles of the nude mice, and bioluminescence was measured periodically. This study was approved by the Ethics Committee of Chinese PLA General Hospital. The animal protocol used in this study was approved by the Ethics Committee of Beijing Institute of Biotechnology.

Statistical analysis

All statistical analyses were performed using GraphPad Crystal 8.0.1 (GraphPad Programming). Data were represented as mean ± SD of three replicate experiments. Analysis of comparisons between bundles was performed using the Student *t* test. The statistical significance is indicated at $P < 0.05$.

Data availability

The sequencing data of this study have been submitted to NGDC, with the accession number HRA007047.

Ethical approval

Studies using human serum and CSF samples were approved by The Second Hospital of Hebei Medical University and performed in accordance with the principles of the Declaration of Helsinki. The animal study was approved by the Animal Ethic Review Committee of Beijing Institute of Biotechnology. All animal experiments were strictly implemented in compliance with the NIH Guide for the Care and Use of Laboratory Animals.

Consent to participate and consent to publish

The patients provided their written informed consent to participate in this study. We have obtained consent to publish this article from all the participants of this study.

Results

Next-generation sequencing of EV miRNA in sera of patients with NSCLC with LM

EVs were purified from serum or CSF by size-exclusion chromatography. TEM and NTA showed that the purified EVs were oval- or bowl-shaped, with sizes ranging from 30 to 150 nm (**Fig. 1A** and **B**). The detection of EV marker proteins by Western blotting (WB) showed that CD63, TSG101, and Alix were enriched in EVs isolated from serum, whereas the EV exclusion marker calnexin was absent (**Fig. 1C**; ref. 19). Taken together, these results confirmed that the main components of the purified microvesicles were exosomes.

A total of 913 miRNAs were detected by next-generation sequencing (NGS) of serum EV RNA in the four groups, 22 of which were differentially expressed ($|\log_2$ fold change$| > 0.8$; $P < 0.05$; **Fig. 1D**). Their target genes were queried in the website, and a total of 6,510 mRNAs were identified as potential targets of these 22 miRNAs (Supplementary Fig. S1A). The Database for Annotation, Visualization, and Integrated Discovery tool was used for Kyoto Encyclopedia of Genes and Genomes enrichment analysis and Gene Ontology functional annotation of the miRNA target genes. Thirty-one pathways in the Kyoto Encyclopedia of Genes and Genomes database were significantly enriched (Supplementary Fig. S1C). The Gene Ontology functional annotations showed enrichment of molecular functions related to neural behaviors, endothelial cells, and positive regulation of endothelial cell migration and cell adhesion (Suppplementary Fig. S1B). In order to identify NSCLC-LM–specific

(*Continued.*) with miR-374a-5p overexpression. Scale bars represent 25 μm. **C** and **D,** Wound healing and Transwell assay detecting the migration and invasion of A549 cells with miR-374a-5p overexpression. **E,** After adding PKH26-labeled EVs derived from 95D cells for 8 hours, PKH26 lipid dye was internalized into hCMEC/D3, whereas the PKH26 dye was rarely seen in HBVPC and HA1800. Scale bars represent 43 μm. **F–H,** Expression of miR-374a-5p in hCMEC/D3, HBVPC, and HA1800 incubated with EVs derived from 95D by qRT-PCR. *, $P < 0.05$; **, $P < 0.01$; ***, $P < 0.001$; ****, $P < 0.001$. NC, normal cells; ns, not significant.

miRNAs, we reclassified the data into NSCLC-LM and non-LM for analysis. Only three NSCLC-LM–specific miRNAs were found. One was upregulated (miR-374a-5p), and the other two were downregulated (miR-3137-5p and miR-370-3P; **Fig. 1E**). Studies have shown that miR-374a-5p is a cancer-promoting factor and that its high expression is often associated with metastasis and poor prognosis (20–22). Therefore, miR-374a-5p was chosen as the target of our research.

The expression of EV miR-374a-5p was detected in serum and CSF

After selecting EV miR-374a-5p as the research factor, we used ddPCR to quantitatively analyze serum EV miR-374a-5p in 106 patients (30 noncancer, 24 early NSCLC, 26 NSCLC, and 26 NSCLC-LM samples). The result displayed that the serum EV miR-374a-5p level was higher in patients with NSCLC-LM than that in non-LM ($P < 0.05$), and there is no significant difference in EV miR-374a-5p levels in noncancer, early, and advanced NSCLC samples. This suggested that EV miR-374a-5p levels were specific to NSCLC-LM (**Fig. 2A**). The analysis of the survival time of patients with NSCLC-LM showed that the level of serum EV miR-374a-5p was negatively correlated with survival time ($P < 0.05$; **Fig. 2B**). We also isolated EVs from the CSF of patients with NSCLC-LM and non-LM (Supplementary Fig. S2A–S2C) and quantified miR-374a-5p levels in EVs of CSF. The level of EV miR-374a-5p in CSF of patients with NSCLC-LM was significantly higher than that in non-LM samples ($P < 0.01$; **Fig. 2C**), and the high level of EV miR-374a-5p in CSF was also negatively correlated with the survival time of patients with NSCLC-LM ($P < 0.01$; **Fig. 2D**). Moreover, we were surprised to find that the EV miR-374a-5p levels in CSF were enriched in patients with NSCLC-LM, and the serum EV miR-374a-5p content of these patients was also rich. The EV miR-374a-5p levels in serum were also low in patients with NSCLC-LM with poor CSF EV miR-374a-5p. These results indicate that EV miR-374a-5p expression was consistent in EVs of CSF and serum in the same patient. We believe that detection of serum biomarkers may replace detection of CSF biomarkers as a diagnostic method for LM ($P < 0.0001$; **Fig. 2E**).

In summary, our data indicated that EV miR-374a-5p levels were specifically abundant in serum and CSF of patients with LM and EV miR-374a-5p levels in serum and CSF of the same patient were consistent. EV miR-374a-5p levels were associated with survival time in patients with NSCLC-LM. We conclude that the detection of serum EV miR-374a-5p may replace CSF as a blood biomarker for the early diagnosis and prognosis of NSCLC-LM. At the same time, the role of miR-374a-5p in the NSCLC-LM process has aroused our interest.

NSCLC-derived EV miR-374a-5p was absorbed by hCMEC/D3 cells

To investigate the role of miR-374a-5p in NSCLC-LM, we first detected its content in EVs extracted from cells and supernatant. miR-374a-5p was quantified in NSCLC cell lines (H1299, A549, 95C, and 95D) and BEAS-2B cells. The results confirmed that miR-374a-5p in lung cancer cells was significantly higher than that in BEAS-2B cells (Supplementary Fig. S3A). EVs from the cell supernatant were extracted and identified (Supplementary Fig. S3B–S3D). The quantitative results showed that the EV miR-374a-5p in NSCLC was significantly higher than that in BEAS-2B cells. This result was consistent with the previous conclusion that tumor cells secrete more EVs than normal cells. Interestingly, miR-374a-5p was most abundant in EVs of highly metastatic lung cancer cells (95D; **Fig. 3A**). We also focused on the function of miR-374a-5p in NSCLC cells. Overexpression of miR-374a-5p enhanced the migration and invasion of lung cancer cells (**Fig. 3C** and **D**) but did not affect cell proliferation (**Fig. 3B**). We suspected that miR-374a-5p may be an essential factor in NSCLC metastasis.

The BBB cannot be circumvented in malignant tumors with LM. Previous experiments have analyzed that miR-374a-5p may be related to endothelial cell function. Therefore, we suspect that miR-374a-5p may affect the BBB. hCMEC/D3, HA1800, and HBVPC cells were selected as potential target cells for the experiment. We cocultured PKH26-labeled EVs (from 95D cells) with cells to find the receptor cells for EVs. It can be clearly observed that all PKH26-labeled EVs are absorbed by hCMEC/D3 cells. However, the fluorescence of PKH26 was almost absent in HA1800 and HBVPC cells (**Fig. 3E**). We extracted RNA from cells which were coincubated with 95D EVs and detected the level of miR-374a-5p. The result displayed that the miR-374a-5p level was significantly increased in hCMEC/D3 cells after incubation with 95D EVs but did not change in HBVPC and HA1800 cells (**Fig. 3F–H**).

These results suggested that miR-374a-5p was enriched in EVs secreted by highly metastatic NSCLC cells and was absorbed by cerebral microvascular endothelial cells through EV transport. We identified cerebral microvascular endothelial cells as the target cells of NSCLC-derived EVs. However, the function of miR-374a-5p after entering cerebral microvascular endothelial cells was unknown, which requires further validation through cell experiments.

miR-374a-5p increased BBB model permeability

Previous experiments have confirmed that cerebral microvascular endothelial cells were the target cells of EV miR-374a-5p released by NSCLC cells. We observed functional changes by overexpression of miR-374a-5p in cerebral microvascular endothelial cells. It was found that overexpression of miR-374a-5p had no significant effects on the proliferation (**Fig. 4A**) and migration (**Fig. 4B** and **C**) of hCMEC/D3 cells. Tube formation assays showed that the cell junction was significantly reduced with miR-374a-5p overexpression in hCMEC/D3 cells (**Fig. 4D**; Supplementary Fig. S4A and S4B). We added the miR-374a-5p inhibitor in the hCMEC/D3 cell tube formation assay. The results showed that hCMEC/D3 cell junctions seemed to increase but were not statistically significant (Supplementary Fig. S4C). We considered that this result may be caused by the low basic miRNA-374a-5p contents in hCMEC/D3 cells, and the effect of reinhibition may not be obvious. In addition, immunofluorescence experiments confirmed that hCMEC/D3 cells have an abnormal distribution of ZO1 and occludin after miRNA-374a-5p overexpression. ZO1 and occludin failed to cluster at the apical interface of cell contacts and lost their zonular distribution (**Fig. 4E**; Supplementary Fig. S4C). The results of WB analysis indicated that miR-374a-5p did not affect ZO1 or occludin expression (Supplementary Fig. S4D).

We used hCMEC/D3 cells and HA1800 cells to construct the BBB model in a 0.4-μm Transwell chamber (Supplementary Fig. S4E). The barrier resistance in the BBB model was 34 to 36 Ω, which was basically consistent with previous experiments (23). The experimental results showed that the overexpression of miR-374a-5p in hCMEC/D3 cells significantly reduced the resistance of the BBB model ($P < 0.0001$; **Fig. 4F**). *In vitro* permeability measurements of rhodamine-labeled dextran (relative molecular weight: 70,000) added to the BBB model showed that hCMEC/D3 cells treated with miR-374a-5p induced more dextran particles from top to bottom of the BBB model ($P < 0.001$; **Fig. 4G**). The 0.8-μm Transwell chamber was used to construct the hCMEC/D3 cell monolayer barrier for tumor cell migration across the endothelial barrier. We found that

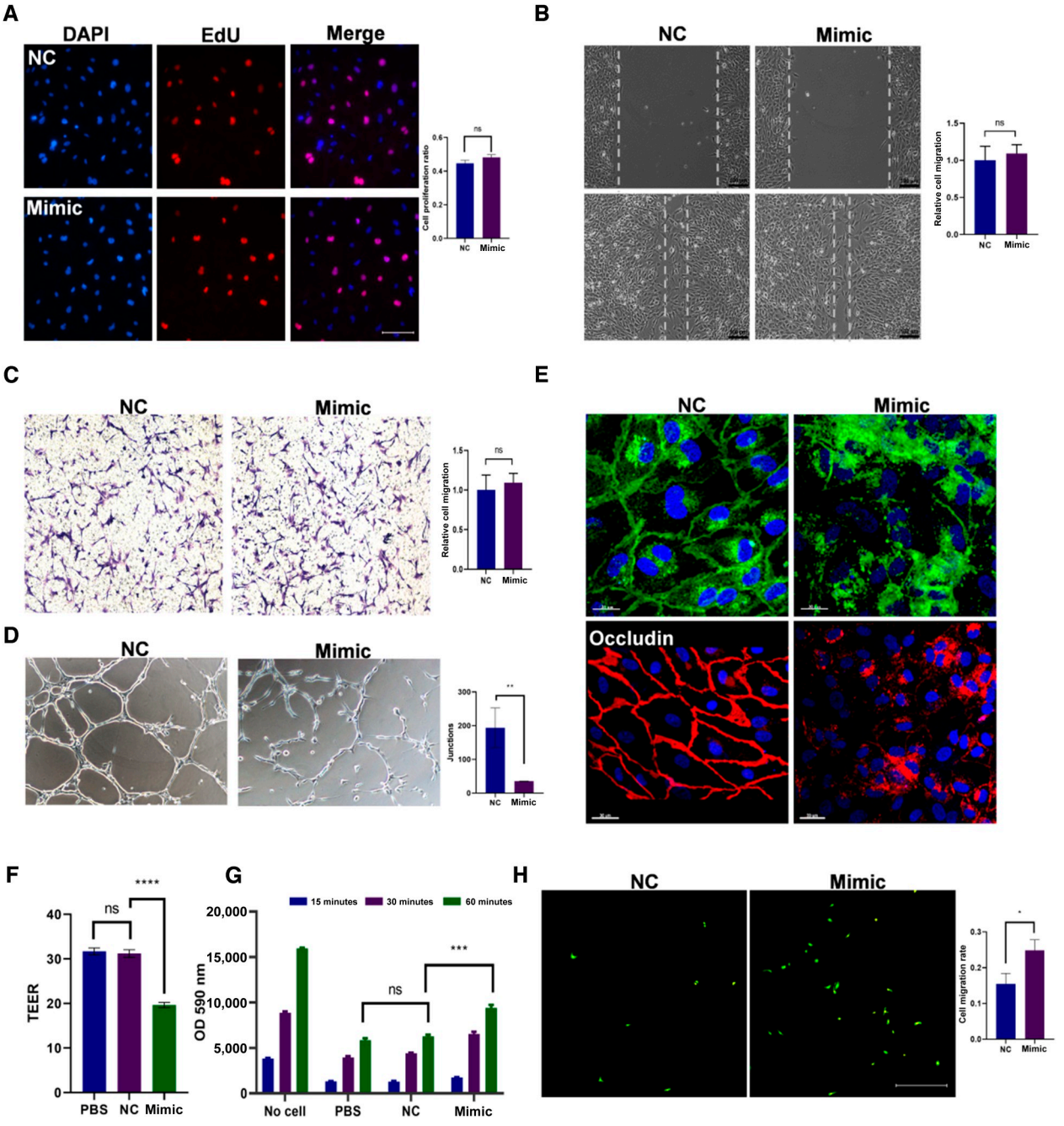

Figure 4.

miR-374a-5p increased BBB model permeability. **A,** EdU assay detecting hCMEC/D3 viability with miR-374a-5p overexpression. Scale bars represent 25 μm. **B** and **C,** Wound healing and Transwell assay detecting the migration of hCMEC/D3 with miR-374a-5p overexpression. **D,** *In vitro* tube forming assay detecting junctions of hCMEC/D3 cells with miR-374a-5p overexpression. **E,** Immunofluorescence staining analysis of ZO1 and occludin expression in hCMEC/D3 with miR-374a-5p overexpression. Scale bars represent 30 μm. **F,** Trans-epithelial electrical resistance (TEER) analysis was performed in the BBB model with miR-374a-5p overexpression. The calculated unit area resistance in triplicate wells was normalized to that in control-treated wells. **G,** Effects of miR-374a-5p overexpression on the permeability of the BBB model after the addition of rhodamine-labeled dextran measured using the *in vitro* permeability assay. **H,** Number of GFP + A549 cells invaded through the hCMEC/D3 monolayers pretreated with miR-374a-5p overexpression. *, $P < 0.05$; **, $P < 0.01$; ***, $P < 0.001$. NC, normal cells; ns, not significant; OD, optical denisty.

miR-374a-5p overexpression in hCMEC/D3 cells caused a substantial increase in the number of A549 cells migrating across the endothelial barrier compared with the control group (**Fig. 4H**). Our experiments showed that BBB model dysfunction and permeability changes resulted from miR-374a-5p influence on tight junction protein distribution in cerebral microvascular endothelial cells. The

mechanism of miR-374a-5p leading to these functional changes had aroused our consideration.

ADD3 was the functional target of miR-374a-5p in hCMEC/D3 cells

miRNAs interacted with the 3′-UTR of target mRNA to induce mRNA degradation and translational repression and regulated gene expression and cell function (24). To further determine the target genes of miR-374a-5p, we used miRDB to predict four candidate genes. qRT-PCR assays found that *ADD3* was negatively related to the expression of miR-374a-5p (**Fig. 5A**). The database predicted three potential binding sites between miR-374a-5p and ADD3 3′-UTR (**Fig. 5B**). We synthesized a luciferase reporter gene plasmid in which the sequence or the mutated sequence containing the putative binding site of miR-374a-5p with the *ADD3* 3′-UTR was fused to the 3′-end of the luciferase sequence. The experiment confirmed the direct binding of *ADD3* to miR-374a-5p in HEK-293 T cells (**Fig. 5C** and **D**). qRT-PCR and WB analyses showed that the expression of *ADD3* was significantly decreased in hCMEC/D3 cells transfected with miR-374a-5p mimics both at mRNA and protein levels, whereas *ADD3* expression was obviously increased in hCMEC/D3 cells transfected with miR-374a-5p inhibitors (**Fig. 5E** and **F**). The immunofluorescence assay showed that *ADD3* and tight junction protein were co-located at the apical interface of cell junctions (Supplementary Fig. S5A).

Rescue experiments were performed by analyzing the over-expression of miR-374a-5p and *ADD3* in hCMEC/D3 cells to confirm their interactions and changes in cellular function. In hCMEC/D3 cells, the tube forming assay showed that *ADD3* could reverse the reduction of hCMEC/D3 cell junctions caused by miR-374a-5p (**Fig. 6A**; Supplementary S6A and S6B). Immunofluorescence staining showed that *ADD3* could resist miR-374a-5p to restore the normal

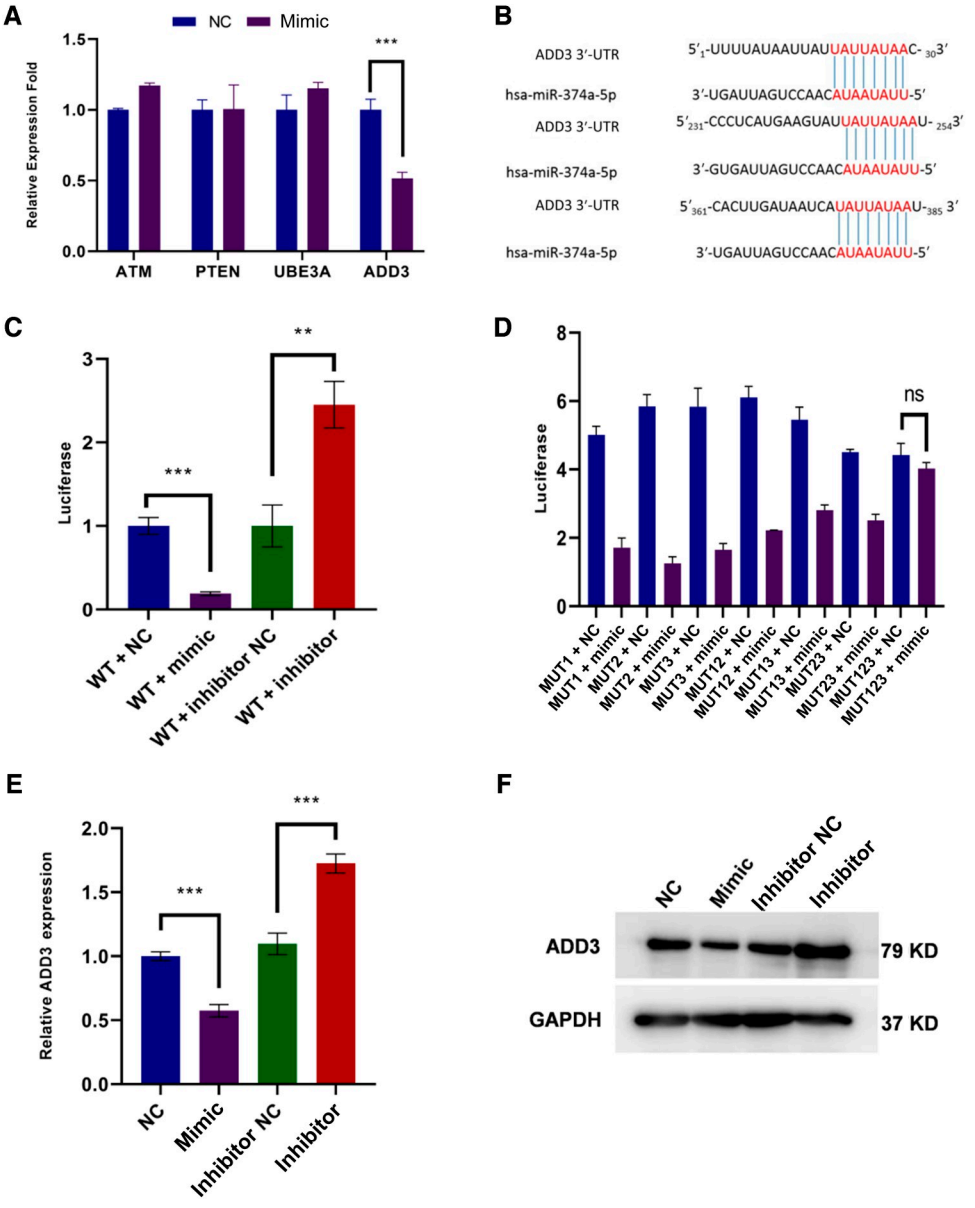

Figure 5.

ADD3 was the functional target of miR-374a-5p in hCMEC/D3 cells. **A,** Potential target genes predicting miR-374a-5p on miRDB by qRT-PCR. **B,** Sequence alignment identified potential binding sites for miR-374a-5p in the 3′-UTR of the ADD3 mRNA. **C,** Luciferase activity in hCMEC/D3 cells transfected with the ADD3 wild-type 3′-UTR vector (WT). **D,** Luciferase activity in hCMEC/D3 cells transfected with the ADD3 mutant 3′-UTR vector (MUT; the miR-374a-5p target sites were mutated). **E** and **F,** WB and qRT-PCR were conducted to determine the expression of ADD3 at both protein and mRNA levels in hCMEC/D3 cells transfected with miR-374a-5p mimic and miR-374a-5p inhibitor. *, $P < 0.05$; **, $P < 0.01$; ***, $P < 0.001$. NC, normal cells; ns, not significant.

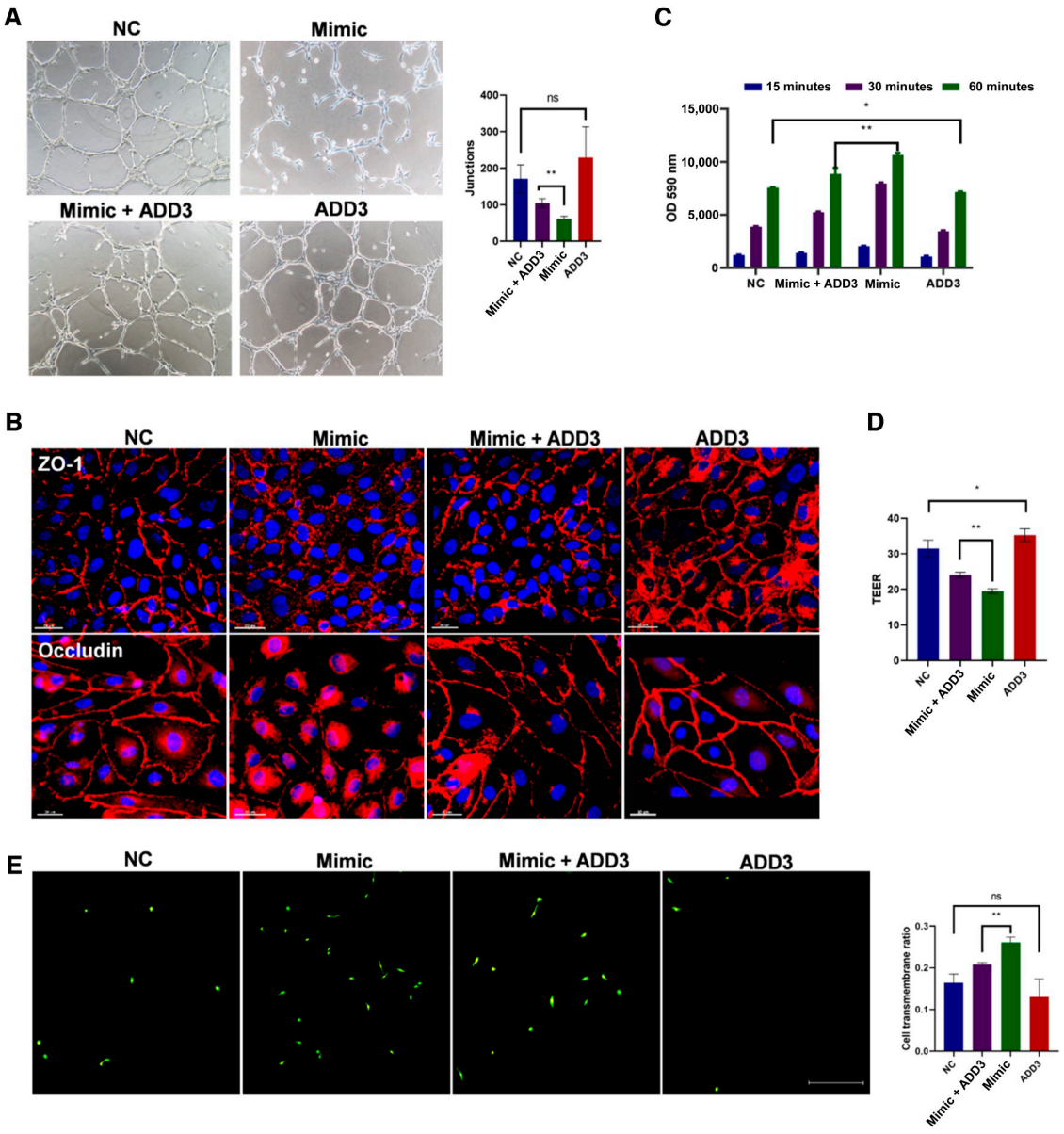

Figure 6.

Rescue experiments. **A,** *In vitro* tube forming assay detecting junctions of hCMEC/D3 cells with *ADD3* or miR-374a-5p and cotransfected with *ADD3* and miR-374a-5p. **B,** Immunofluorescence staining analysis of ZO1 and occludin expression in hCMEC/D3 cells with *ADD3* or miR-374a-5p and cotransfected with *ADD3* and miR-374a-5p. Scale bars represent 30 μm. **C,** Effects of *ADD3* or miR-374a-5p and cotransfection with *ADD3* and miR-374a-5p on the permeability of the BBB model after the addition of rhodamine-labeled dextran measured using the *in vitro* permeability assay. **D,** Trans-epithelial electrical resistance (TEER) analysis was performed in the BBB model with *ADD3* or miR-374a-5p and cotransfected with *ADD3* and miR-374a-5p. **E,** Number of GFP + A549 cells invaded through the hCMEC/D3 monolayers pretreated with *ADD3* or miR-374a-5p and cotransfected with *ADD3* and miR-374a-5p. *, $P < 0.05$; **, $P < 0.01$; ***, $P < 0.001$. NC, normal cells; ns, not significant; OD, optical density.

distribution of ZO1 and occludin in hCMEC/D3 cells (**Fig. 6B**). In the BBB model, *ADD3* eliminated the decreased barrier function caused by miR-374a-5p (**Fig. 6D**) and reduced permeability (**Fig. 6C**). After pretreating the hCMEC/D3 monolayer with *ADD3* and miR-374a-5p, the number of GFP-labeled A549 cells invaded through the barrier was significantly reduced compared with miR-374a-5p (**Fig. 6E**). The above results suggested that *ADD3* was the functional target of miR-374a-5p in hCMEC/D3 cells.

NSCLC-derived EV miR-374a-5p promotes LM *in vitro* and *in vivo*

To demonstrate the role of NSCLC-derived EV miR-374a-5p, we constructed 95D cells that overexpressed miR-374a-5p, and the EVs overexpressed miR-374a-5p were isolated from the cell supernatant which was named 95D EV miR-374a-5p (Supplementary Fig. S7A). The qRT-PCR assays showed that the level of miR-374a-5p in hCMEC/D3 cells was significantly increased after absorption of 95D EV miR-374a-5p (Supplementary Fig. S7B). WB

confirmed that 95D EV miR-374a-5p decreased *ADD3* protein levels in hCMEC/D3 cells (Supplementary Fig. S7C). Similar to the induction effect of miR-374a-5p in hCMEC/D3 cells, 95D EV miR-374a-5p also resulted in decreased cell junctions in hCMEC/D3 cells (**Fig. 7A**; Supplementary Fig. S7D and S7E). The changes in resistance (**Fig. 7B**) and permeability (**Fig. 7C**) of 95D EV miR-374a-5p in the BBB model were more serious than those in 95D EVs. Compared with the control groups, the number of GFP + A549 cells invaded through the

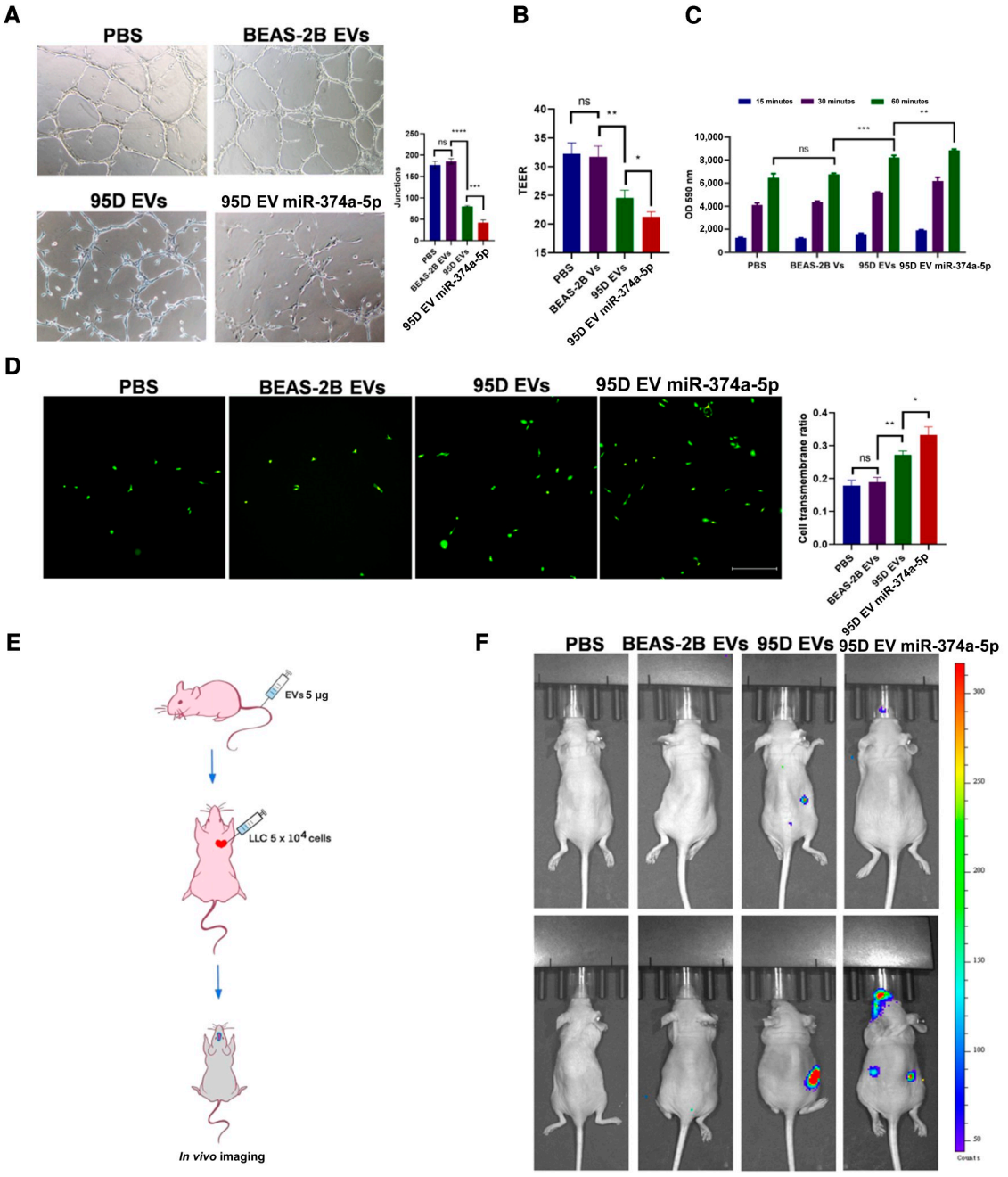

Figure 7.

EV miR-374a-5p promotes NSCLC cell metastasis *in vitro* and *in vivo*. **A,** *In vitro* tube forming assay detecting junctions of hCMEC/D3 cells with PBS, BEAS-2B EVs, 95D EVs, and 95D EV miR-374a-5p. **B,** Trans-epithelial electrical resistance (TEER) analysis was performed in the BBB model with PBS, BEAS-2B EVs, 95D EVs, and 95D EV miR-374a-5p. **C,** Effects of PBS, BEAS-2B EVs, 95D EVs, and 95D EV miR-374a-5p on the permeability of the BBB model after the addition of rhodamine-labeled dextran measured using the *in vitro* permeability assay. **D,** Number of GFP + A549 cells invaded through the hCMEC/D3 monolayers pretreated with PBS, BEAS-2B EVs, 95D EVs, and 95D EV miR-374a-5p. **E,** An *in vivo* model was established. EVs were injected into nude mice through the tail vein for pretreatment for 2 weeks, and LLC was injected into the left ventricle of mice to simulate circulating tumor cells. **F,** *In vivo* imaging for LM in nude mice injected with PBS, BEAS-2B EVs, 95D EVs, and 95D EV miR-374a-5p. *, $P < 0.05$; **, $P < 0.01$; ***, $P < 0.001$; ns, not significant; OD, optical density.

hCMEC/D3 monolayer was significantly increased because of the addition of 95D EV miR-374a-5p (**Fig. 7D**).

In *in vivo*, 95D EV miR-374a-5p was injected into nu/nu nude mice via the tail vein, and BEAS-2B EVs and unmodified 95D EVs were used as controls. Two weeks after EV injection, LLCs were injected into the left ventricle of mice (**Fig. 7E**). Head images of nude mice were observed using *in vivo* imaging techniques. The results showed that 3 days after LLC injection, *in vivo* imaging of the head of mice injected with 95D EV miR-374a-5p revealed LM, whereas no LM was observed in the control groups. Seven days after injection, the *in vivo* imaging of the head of mice injected with 95D EV miR-374a-5p showed the occurrence of more obvious LM than that observed previously, whereas no LM was observed in the control groups (**Fig. 7F**).

These results indicate that NSCLC-derived EVs carry miR-374a-5p into cerebral microvascular endothelial cells to regulate *ADD3*, which caused cell junction reduction and BBB dysfunction and contributed to the progression of NSCLC to LM *in vivo*.

Discussion

Currently, lung cancer still ranks highly among cancers in terms of global morbidity and mortality. Despite the prolonged survival of patients with lung cancer, the incidence of LM has been increasing in recent years (25). Recently, studies on LM have received more attention. For example, Boire and colleagues found that cancer-derived complement component 3 disrupts the blood–CSF barrier, allowing nutrients to enter the CSF and promoting cancer cell growth (26). The rare cell capture technique can be used to detect LM. LM diagnosis by counting circulating tumor cells in CSF is more specific and sensitive than routine CSF cytology and radiologic studies (27, 28). However, the diagnosis of LM was still not unsatisfactory, and there is an urgent need for better molecular markers.

Accumulating evidence has revealed that EV-associated miRNAs extracted from the body fluids of patients with cancer can be recognized as new diagnostic and prognostic biomarkers and as therapeutic targets (29). In the LM studies, the related EV miRNAs have received attention. Lee obtained a comprehensive RNA expression profile using 472 CSF samples derived from patients with LM and found that the elevated concentration of EV miRNA-21 in CSF of patients with LM may be a predictive marker for survival duration (30). Three highly expressed miRNAs (miR-183-5p, miR-96-5p, and miR-182-5p) in CSF EVs can be used as biomarkers for diagnosing or monitoring the progression of NSCLC-LM (31). Our experiment proved that EV miR-374a-5p was not only highly expressed in sera of patients with NSCLC-LM but also enriched in the CSF of same patients, and even the EV miR-374a-5p level was correlated with the survival time. We believed that EV miR-374a-5p may be a biomarker for the diagnosis and prognosis of NSCLC-LM.

Brain microvascular endothelial cells and the surrounding accompanying cells constitute the BBB. The endothelial cells and pericytes are surrounded by a basement membrane, and the astrocyte endfeet ensheathe at the abluminal side of the capillaries with a coverage estimated at 99%. Both pericytes and astrocytes regulate the phenotype of the endothelium and play a supporting role in the BBB. The brain microvascular endothelial cells constitute the capillary wall and thus act as the actual barrier (32). The tight junctions are present at the sites of fusion of adjacent endothelial cells. The observed barrier dysfunction was mainly due to changes in BBB permeability (resulting from tight junction opening; ref. 33).

Exosome-mediated transfer of miRNAs between cancer cells and stromal cells is essential for cancer progression (34). Exosomal miRNAs can promote cancer metastasis by regulating the function of vascular endothelial cells (35). It was recently reported that exosome-mediated transfer of cancer cell–derived miR-105 into vascular endothelial cells promotes cancer progression by targeting ZO1 and effectively disrupting tight junctions and the integrity of the related natural barriers (36). Colorectal cancer–derived exosome miR-25-3p is involved in premetastatic niche formation (37). Our results showed that miR-374a-5p in EVs secreted by NSCLC transferred to brain microvascular endothelial cells promoted the internalization of tight junction proteins (ZO1 and occludin) by targeting *ADD3*, which resulted in decreased permeability of BBB and ultimately promoted NSCLC-LM.

Studies have revealed that tumor-derived exosomes frequently transfer miRNAs to recipient cells to induce repression of target genes (38). Our study confirmed that *ADD3* was the direct target of miR-374a-5p in brain microvascular endothelial cells. Adducin was an assembly factor participating in the formation of the spectrin–actin membrane skeleton and is involved in cytoskeletal network formation, cellular signal transduction, ion transport, cell motility, and cell proliferation (39, 40). It has long been recognized that *ADD1* and *ADD3* are enriched at intercellular junctions *in vivo* (41).The phosphorylated form of adducin plays important roles in localizing junctions (42). Studies have shown that in *ADD*-deficient cells, large amounts of E-cadherin and β-catenin remain in the cytoplasm and do not reach the cell contact, forming only short defective tight junctions (43). Our study showed that NSCLC-derived EV miR-374a-5p regulates the distribution of ZO1 and occludin in brain microvascular endothelial cells by directly targeting *ADD3*. Downregulation of *ADD3* results in abnormal distribution of ZO1 and occludin in hCMEC/D3 cells, leading to increased BBB permeability and promoting NSCLC-LM.

In summary, our study elucidates that NSCLC-derived EV miR-374a-5p can be transferred to brain microvascular endothelial cells and thereby promoted BBB permeability by directly regulating *ADD3*. Finally, our data suggested that serum EV miR-374a-5p may be a blood biomarker for early diagnosis and prognosis of NSCLC-LM.

Authors' Disclosures

No disclosures were reported.

Authors' Contributions

J. Jin: Data curation, software, formal analysis, supervision, funding acquisition, writing–original draft, project administration, writing–review and editing. **Y. Cui:** Data curation, software, methodology. **H. Niu:** Data curation, validation, investigation. **Y. Lin:** Data curation, software, formal analysis, visualization, methodology. **X. Wu:** Data curation, software, visualization, methodology. **X. Qi:** Data curation, investigation. **K. Bai:** Data curation, investigation. **Y. Zhang:** Data curation, investigation. **Y. Wang:** Conceptualization, resources, data curation, software, formal analysis, methodology, project administration, writing–review and editing. **H. Bu:** Conceptualization, resources, data curation, formal analysis, funding acquisition, writing–review and editing.

Acknowledgments

This work was supported by the National Key Research and Development Program (2019YFA0903800 and 2022YFC3600100) and Natural Science Foundation of Hebei Province of China (No. H2020206126).

Note

Supplementary data for this article are available at Molecular Cancer Research Online (http://mcr.aacrjournals.org/).

Received January 15, 2024; revised February 27, 2024; accepted April 16, 2024; published first April 19, 2024.

References

1. Raizer J, Hwu W, Panageas K, Wilton A, Baldwin D, Bailey E, et al. Brain and leptomeningeal metastases from cutaneous melanoma: survival outcomes based on clinical features. Neuro Oncol 2008;10:199–207.
2. Remon J, Le Rhun E, Besse B. Leptomeningeal carcinomatosis in non-small cell lung cancer patients: a continuing challenge in the personalized treatment era. Cancer Treat Rev 2017;53:128–37.
3. Li Y, Jiang B, Yang J, Tu H, Zhou Q, Guo W, et al. Leptomeningeal metastases in patients with NSCLC with EGFR mutations. J Thorac 2016;11:1962–9.
4. Lamba N, Wen P, Aizer A. Epidemiology of brain metastases and leptomeningeal disease. Neuro Oncol 2021;23:1447–56.
5. Wang Y, Yang X, Li N, Xue J. Leptomeningeal metastases in non-small cell lung cancer: diagnosis and treatment. Lung Cancer 2022;174:1–13.
6. Davis P, Friedman N, Fry S, Malko J, Hoffmann J, Braun I. Leptomeningeal metastasis: MR imaging. Radiology 1987;163:449–54.
7. Pan Z, Yang G, He H, Yuan T, Wang Y, Li Y, et al. Leptomeningeal metastasis from solid tumors: clinical features and its diagnostic implication. Sci Rep 2018;8:10445.
8. Fischer S, Weber J, Senn-Schönenberger I, Cerny T, Hundsberger T. Neuroborreliosis mimicking leptomeningeal carcinomatosis in a patient with breast cancer: a case report. J Invest Med High Impact Ccase Rep 2014;2: 2324709614529417.
9. Saltijeral S, Grosu H, De La Garza H, O'Brien B, Iliescu G. Leptomeningeal enhancement due to neurosarcoidosis mimicking malignancy. Case Rep Med 2020;2020:9513576.
10. Le Rhun E, Devos P, Seystahl K, Jongen J, Gramatzki D, Roth P, et al. Prognostic role of ventricular size and its dynamics in patients with leptomeningeal metastasis from solid tumors. Neurology 2024;102:e207959.
11. Kalluri R, McAndrews K. The role of extracellular vesicles in cancer. Cell 2023; 186:1610–26.
12. Clancy J, D'Souza-Schorey C. Tumor-derived extracellular vesicles: multifunctional entities in the tumor microenvironment. Annu Rev Pathol 2023;18:205–29.
13. Shah R, Patel T, Freedman J. Circulating extracellular vesicles in human disease. N. Engl J Med 2018;379:958–66.
14. Urabe F, Patil K, Ramm G, Ochiya T, Soekmadji C. Extracellular vesicles in the development of organ-specific metastasis. J Extracell Vesicles 2021;10:e12125.
15. Xu Z, Liu X, Wang H, Li J, Dai L, Li J, et al. Lung adenocarcinoma cell-derived exosomal miR-21 facilitates osteoclastogenesis. Gene 2018;666:116–22.
16. Li C, Qin F, Wang W, Ni Y, Gao M, Guo M, et al. hnRNPA2B1-mediated extracellular vesicles sorting of miR-122-5p potentially promotes lung cancer progression. Int J Mol Sci 2021;22:12866.
17. Geng S, Tu S, Bai Z, Geng Y. Exosomal lncRNA LINC01356 derived from brain metastatic nonsmall-cell lung cancer cells remodels the blood-brain barrier. Front Oncol 2022;12:825899.
18. He F, Zhong X, Lin Z, Lin J, Qiu M, Li X, et al. Plasma exo-hsa_circRNA_ 0056616: a potential biomarker for lymph node metastasis in lung adenocarcinoma. J Cancer 2020;11:4037–46.
19. Wang X, Tian L, Lu J, Ng I. Exosomes and cancer—diagnostic and prognostic biomarkers and therapeutic vehicle. Oncogenesis 2022;11:54.
20. Han T, Zhuo M, Yuan C, Xiao X, Cui J, Qin G, et al. Coordinated silencing of the Sp1-mediated long noncoding RNA MEG3 by EZH2 and HDAC3 as a prognostic factor in pancreatic ductal adenocarcinoma. Cancer Biol Med 2020; 17:953–69.
21. Son D, Kim Y, Lim S, Kang H, Kim D, Park J, et al. miR-374a-5p promotes tumor progression by targeting ARRB1 in triple negative breast cancer. Cancer Lett 2019;454:224–33.
22. Ji R, Zhang X, Gu H, Ma J, Wen X, Zhou J, et al. miR-374a-5p: a new target for diagnosis and drug resistance therapy in gastric cancer. Mol Ther Nucleic Acids 2019;18:320–31.
23. Srinivasan B, Kolli A, Esch M, Abaci H, Shuler M, Hickman J. TEER measurement techniques for in vitro barrier model systems. J Lab Autom 2015;20:107–26.
24. Slack F, Chinnaiyan A. The role of non-coding RNAs in oncology. Cell 2019; 179:1033–55.
25. Ozcan G, Singh M, Vredenburgh J. Leptomeningeal metastasis from non-small cell lung cancer and current landscape of treatments. Clin Cancer Res 2023;29: 11–29.
26. Boire A, Zou Y, Shieh J, Macalinao D, Pentsova E, Massagué J. Complement component 3 adapts the cerebrospinal fluid for leptomeningeal metastasis. Cell 2017;168:1101–13.e13.
27. Lin X, Fleisher M, Rosenblum M, Lin O, Boire A, Briggs S, et al. Cerebrospinal fluid circulating tumor cells: a novel tool to diagnose leptomeningeal metastases from epithelial tumors. Neuro Oncol 2017;19:1248–54.
28. Nayak L, Fleisher M, Gonzalez-Espinoza R, Lin O, Panageas K, Reiner A, et al. Rare cell capture technology for the diagnosis of leptomeningeal metastasis in solid tumors. Neurology 2013;80:1598–605. discussion 603.
29. Wang D, Zhang W, Zhang C, Wang L, Chen H, Xu J. Exosomal non-coding RNAs have a significant effect on tumor metastasis. Mol Ther Nucleic Acids 2022;29:16–35.
30. Lee K, Im J, Lin W, Gwak H, Kim J, Yoo B, et al. Nanoparticles in 472 human cerebrospinal fluid: changes in extracellular vesicle concentration and miR-21 expression as a biomarker for leptomeningeal metastasis. Cancers (Basel) 2020; 12:2745.
31. Li H, Xia M, Zheng S, Lin Y, Yu T, Xie Y, et al. Cerebrospinal fluid exosomal microRNAs as biomarkers for diagnosing or monitoring the progression of non-small cell lung cancer with leptomeningeal metastases. Biotechnol Genet Eng Rev 2023;1–22.
32. Helms H, Abbott N, Burek M, Cecchelli R, Couraud P, Deli M, et al. In vitro models of the blood-brain barrier: an overview of commonly used brain endothelial cell culture models and guidelines for their use. J Cereb Blood flow 2016;36:862–90.
33. Obermeier B, Daneman R, Ransohoff R. Development, maintenance and disruption of the blood-brain barrier. Nat Med 2013;19:1584–96.
34. Zhao S, Mi Y, Zheng B, Wei P, Gu Y, Zhang Z, et al. Highly-metastatic colorectal cancer cell released miR-181a-5p-rich extracellular vesicles promote liver metastasis by activating hepatic stellate cells and remodelling the tumour microenvironment. J Extracell Vesicles 2022;11:e12186.
35. Fang J, Zhang Z, Shang L, Luo Y, Lin Y, Yuan Y, et al. Hepatoma cell-secreted exosomal microRNA-103 increases vascular permeability and promotes metastasis by targeting junction proteins. Hepatology 2018;68:1459–75.
36. Zhou W, Fong M, Min Y, Somlo G, Liu L, Palomares M, et al. Cancer-secreted miR-105 destroys vascular endothelial barriers to promote metastasis. Cancer cell 2014;25:501–15.
37. Zeng Z, Li Y, Pan Y, Lan X, Song F, Sun J, et al. Cancer-derived exosomal miR-25-3p promotes pre-metastatic niche formation by inducing vascular permeability and angiogenesis. Nat Commun 2018;9:5395.
38. Cao L, Yang X, Chen Y, Zhang D, Jiang X, Xue P. Correction to: exosomal miR-21 regulates the TETs/PTENp1/PTEN pathway to promote hepatocellular carcinoma growth. Mol Cancer 2020;19:59.
39. Kiang K, Zhang P, Li N, Zhu Z, Jin L, Leung G. Loss of cytoskeleton protein ADD3 promotes tumor growth and angiogenesis in glioblastoma multiforme. Cancer Lett 2020;474:118–26.
40. Langer W, Sohler F, Leder G, Beckmann G, Seidel H, Gröne J, et al. Exon array analysis using re-defined probe sets results in reliable identification of alternatively spliced genes in non-small cell lung cancer. BMC genomics 2010;11: 676.
41. Kaiser HW, O'Keefe E, Bennett V. Ca^{++}-dependent association with sites of cell-cell contact. J Cell Biol 1989;109:557–69.
42. Kugelmann D, Waschke J, Radeva M. Adducin is involved in endothelial barrier stabilization. PLoS One 2015;10:e0126213.
43. Naydenov N, Ivanov A. Adducins regulate remodeling of apical junctions in human epithelial cells. Mol Biol Cell 2010;21:3506–17.